Creep Properties of Alkali-Activated Concrete

Zuhua Zhang, Zhengning Zhou, Susan A. Bernal, Zhenming Li, Patricia Kara De Maeijer, Albina Kostiuchenko, Arkamitra Kar, and Guang Ye

Abstract Concrete is an ageing viscoelastic material exhibiting both elastic (instantaneous) as well as viscous (time-dependent) deformation under loading conditions (either external or internal). There is a limited number of studies focused on the time-dependent response of alkali-activated concretes (AACs) under loading/unloading conditions. Creep of AAC is a complex phenomenon, which is influenced by exposure conditions of the material, including the loading magnitude, temperature, relative humidity, thermal and drying histories; as well as chemical composition and phase assemblages (e.g., type and amount of reaction products) present in the cementitious matrix. AAC has shown very vibrable creep behaviors, due to different raw materials and processes using during their production. Creep studies on room temperature cured slag-based AAC usually show high creep; however, creep studies of different AACs, including fly ash-based and fly ash-slag-blended, indicate that elevated temperature curing could be a suitable mitigation strategy for reducing creep. This is associated with the development of a more mature microstructure in the material, due to an accelerated reaction kinetics and a consequent increase in strength and lower creep. However, applying a curing temperature above 80 °C causes thermal defects

Z. Zhang (✉) · Z. Zhou
Key Laboratory of Advanced Civil Engineering Materials of Ministry of Education, School of Materials Science and Engineering, Tongji University, Shanghai, China
e-mail: zhangzuhua@tongji.edu.cn

S. A. Bernal
School of Civil Engineering, University of Leeds, Leeds, UK

Z. Li
School of Intelligent Civil and Ocean Engineering, Harbin Institute of Technology, Shenzhen, China

P. Kara De Maeijer
Faculty of Applied Engineering, University of Antwerp, Antwerp, Belgium

A. Kostiuchenko · G. Ye
Section Materials and Environment, Department of 3Md, Faculty of Civil Engineering and Geosciences, Delft University of Technology, Delft, The Netherlands

A. Kar
Department of Civil Engineering, Indian Institute of Technology Hyderabad, Sangareddy, India

G. Ye and F. Dehn (eds.), *Mechanical Properties of Alkali-Activated Materials*, RILEM State-of-the-Art Reports 46, https://doi.org/10.1007/978-3-032-07116-3_11

and cracks which increases the creep. For most aluminosilicate-based AACs that produced with fly ash, metakaolin and their blends with a small amount of ground granulated blast furnace slag, the recommended curing method is to use thermal curing at about 60 °C. In addition, curing time and initial loading time are also important. It must be noted that because of the complexity of raw materials properties and mix proportions, there is no universal method for all types of AACs. The existing creep prediction models for Portland cement-based concretes cannot be transferred and adopted in AACs directly due to the distinct nature of hydration products. Therefore, more studies investigated the creep at both small size and full-scale of AACs are urgently needed.

Keywords Alkali-activated concrete (AAC) · Creep · Creep models · Curing conditions · Loading conditions

1 Introduction

Determination of the service life of durable and sustainable concrete structures, particularly long-span, high-value assets such as bridges, high-rise buildings, or structures including tunnels, and dams is an essential part of construction works. It is motivated by the need to ensure the safety of such structures, and by reducing the costs associated with necessary maintenance, repair, or replacement activities after eventual failure. The role of durability in the sustainability of concrete structures is also very prominent. This is associated with the significant reduction of resource consumption that can be achieved by extending the service life of assets for their potential refurbishing or repurposing. Additionally, it acts as a key enabler for the adoption of circular practices including the reuse of structural concrete components, when dismantling or demolishing of a given structure is unavoidable.

The durability of concrete structures is strongly dependent on the intrinsic physicochemical properties of the concrete and the stresses posed by the in-service environment. Extensive research has been conducted to evaluate the chemical durability of concrete specimens [1], including those produced with alkali-activated binders [2, 3]. However, limited information is reported about the effect of loading on the durability performance of concrete structures. The effect of exposure to chlorides [4] and carbonation [5] in the performance of concretes under loading are reported in the literature. However, there is a knowledge gap in terms of development of testing methods for assessing the long-term coupled effect of chemical and loading stresses on concrete durability and deformation. Hence, it is of great importance to understand the deformations that are experienced by structural concrete during its service life.

Creep is the deformation process a material undergoes when subjected to constant loading. Depending on the stiffness of a given concrete and the degree of deformation experienced, creep can cause significant structural damage [6]. The integrity of the structure is not compromised when an acceptable level of creep occurs; however,

the macro- or micro-cracking induced by the progressive deformation can accelerate the deterioration of the concrete. This is associated with the fact that cracks act as conduits facilitating the ingress of aggressive substances into the materials, triggering a variety of durability phenomena [7].

The prediction of concrete creep and the design of concrete structures accounting for such phenomenon is based on empirical experience and long-standing principles and assumptions. Concrete creep, in general, is not a fully understood phenomenon, even for Portland cement (PC) concrete. Consequently, it is not possible reliably to predict or account for creep when designing a given concrete structure [8]. It is in fact a great challenge to design concrete mixes for a minimum creep without overdesigning to compensate the potential deformation.

The binder is the only component in concrete that undergoes deformation. There is extensive information available on the deformation of concrete made with Portland cement. However, it is not suitable to apply the relevant deformation knowledge to alkali-activated concrete (AAC). This is primarily due to the significant differences in the chemistry of alkali-activated materials (AAMs) and Portland cement. The existing reports at the binder scale are limited to evaluating the potential creep of the calcium silicate hydrate (C–S–H) matrix, the primary strength-producing phase in hydrated PC [9]. The addition of aluminosilicate-rich supplementary cementitious materials (SCMs) to PC leads to the formation of a calcium aluminosilicate hydrate (C–A–S–H) matrix in addition to C–S–H. The chemical structure, composition, and mechanical behavior of the C–A–S–H matrix are different from that of C–S–H [10, 11]. In the case of AAMs, those produced with Ca-rich precursors form an alkaline complex matrix of calcium-sodium aluminosilicate, C–(N)–A–S–H [12]. In contrast, the use of low-Ca precursors leads to the formation of a sodium aluminosilicate hydrate (N–A–S–H) matrix, as discussed in Chap. "Conventional Precursors and Activators". The micromechanics of these phases differ significantly, and it is reported that the elastic modulus of individual hardened phases follows an order of N–A–S–H < C–(N)–A–S–H < C–A–S–H [13], for specific paste mixture under identical curing conditions.

For PC systems, it has been identified that the pore structure strongly influences the internal relative humidity, and consequently the autogenous deformation of concrete subjected to loading [6]. The intrinsic differences in the reaction products formed in AAMs lead to changes in transport properties, particularly the pore structure [14]. Therefore, it can be expected that AAC will perform differently under loading, compared to PC concrete. Hence, this chapter reviews the creep deformation of AAC, whereas, the shrinkage behavior reported in previous literature [15] is discussed in detail in Chap. "Autogenous Shrinkage of Alkali-Activated Materials".

In the following sections of this chapter, an overview of studies reporting the creep behavior of AAC is presented, including the factors influencing the performance of these materials, the mechanisms of creep, and the approaches to develop models for predicting the creep behavior of structural concrete made with AAMs.

2 Factors Affecting the Creep of AAC

2.1 Raw Materials

As discussed in previous chapters there is a wide variety of precursors that can be used for producing AAMs, the most commonly used being class F fly ash (FA) and ground granulated blast furnace slag (GGBFS). The specific microstructural features of materials produced with these precursors are discussed in detail in Chap. "Conventional Precursors and Activators", where it is clear that the differences in chemical compositions, specific surface areas, will lead to different reactivities (specific reactivity also depends on the activator type and curing conditions), consequently leading to formation of distinctive features of hardened products [16]. These variations mean that the properties of the AAMs will change depending on the type of precursor used, including the creep behavior of the resultant concrete mixes. In the following sections an overview of the creep results reported for different type of raw materials are discussed.

Fly ash based AAC (FA-based AAC)

FA is widely used in various civil engineering applications as a mineral admixture and SCM. Ye et al. [17] and Harinadha Reddy and Ramaswamy [18] reported that adding a small amount (16–30 wt.%) of FA to PC concrete can effectively reduce the creep deformation. This is mainly attributed to the pozzolanic reaction and improved workability when FA particles are introduced, refining the pore structure, forming a more uniform and dense microstructure, effectively reducing creep deformation of concrete [19].

The reaction mechanism of FA-based AAC and FA-mixed PC concrete is different as discussed in Chap. "Conventional Precursors and Activators". Wallah and Hardjito summarized in a book chapter [20] about their own study on the creep behavior of FA-based AAC and pointed out that the creep strains in FA-based AAC are lower than in ordinary Portland cement concretes, when a comparable range of strength and loading period are considered between the two types of concretes. Sagoe-Crentsil et al. [21] compared the creep characteristics of PC concrete and a steam-cured (65 °C for 6 h followed by 23 °C 100% RH curing) low-Ca FA-based AAC with compressive strength of 44.0 MPa at 28 days. The loading was commenced after 2 days and readjusted after 7 and 28 days at a stress corresponded to 40% of the compressive strength of the concrete mixtures all the time. After loading for 365 days and ageing under the same conditions, the creep coefficient of PC concrete (38.1 MPa at 28 days) was about 1.75, while that of FA-based AAC was about 0.668, which is 45% lower. Davidovits [22] reported that the reduced creep of FA-based AAC is due to the mechanism of "block aggregation". The silicate and alumina components in FA are not fully reacted with the alkali activator, and the "polymerization" that occurs on the surface of the atoms is sufficient to produce the "block" required for the binder. Thus, the unreacted FA particles in the interior part of the AAM remain in stable state to act as "micro-aggregates" in the binder matrix. Figure 1 shows that unreacted and

partially reacted FA particles in the matrix. The surface of the FA particles dissolves and react to form gel, which binds a large number of isolated FA particles, together with a large number of crystalline phases (mullite) from the remained part of FA. All these together combined to form a binder matrix. From the microstructure, it is evident that the nature of FA will affect the creep behavior of the alkali activated binder, consequently the resultant concrete.

A study by Gunasekera et al. [24] compared the creep behavior of AAC prepared with three different FA, with PC concrete over a loading period of 365 days. It must be noted that the curing methods were different: AAC were cured at room temperature for 1 day, then 80 °C oven conditions for 24 h, cooled until room temperature, demolded, followed by room temperature curing until testing; PC concrete were cured at room temperature for 1 day, demolded, followed by water curing at room temperature until testing. Table 1 shows the main chemical composition of the FA sourced from three Australian power stations. Table 1 also shows that, the 28-day compressive strength values (35.6–40.5 MPa) of Gladstone and Pt Augusta FA-based

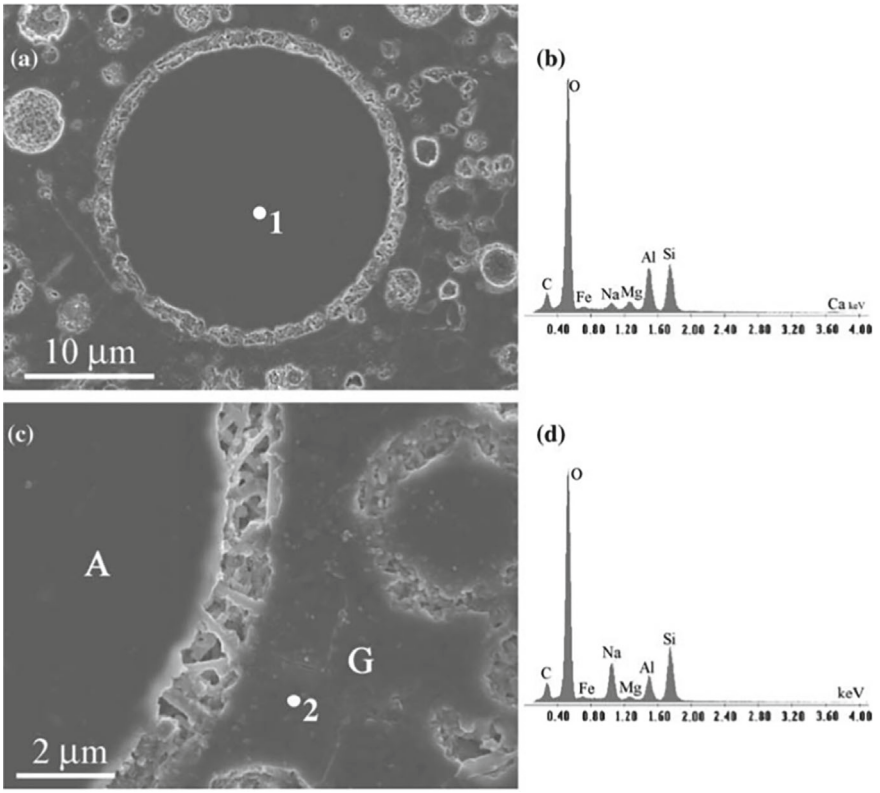

Fig. 1 Typical scanning electron microscope images of a polished section of alkali-activated FA paste. Reproduced from [23]

AACs are comparable to the PC concrete for 36.6 MPa, whereas the Tarong FA-based AAC exhibits much lower strength. Figure 2 shows the creep coefficients of these concrete mixes over a loading period of 365 days. The loading method was the same: applying 40% of the compressive strength of each mixture as the sustained load, in a humidity chamber at 50% relative humidity at 23 ± 2 °C. The early creep of FA-based AAC is lower than the PC concrete. After 365 days, the creep coefficients of the Gladstone and Pt Augusta FA-based AACs are similar. The creep coefficient of the PC concrete is about 40% higher than these values, while the creep coefficient of Tarong FA-based AAC is about twice that of the other two FA-based AAC specimens. These observations confirm that the creep coefficient of FA-based AAC is generally lower than that of PC concrete with the same strength grade, at this specimen preparation conditions. It is noted that, like PC concrete, the creep coefficient of AAC decreases with the increase of 28-day compressive strength.

Figure 3 shows the formation of the hardened matrix and the morphological development from 28 to 365 days in the corresponding binder samples made with the three different FA. The three fly ashes contain large quantity of reactive amorphous alumina and silica components (glass).

In the study by Gunasekera et al. [24], it was found that Gladstone FA had the largest surface area and reacted rapidly under the alkali activation conditions to generate large quantities of N–A–S–H gel. Calcium oxide in the fly ash reacted to form C–A–S–H gel, which diffused throughout the hardened paste, covering and binding the unreacted and partially reacted FA particles together, effectively filling the interior space. Although the higher calcium oxide content of Pt Augusta FA could react to generate more C–A–S–H, the surface area of FA was too small, so the chemical reaction rate and degree of reaction were low. Although Tarong FA had larger surface area, the chemistry of FA did not give enough reactive components to form gels, therefor, at 28 days, the hardened binder was loose, and the compressive strength was lower. Over time, FA continued to dissolve, producing more gel, so a significant increase in the compressive strength of Tarong FA-based AAC was observed at 365 days.

The study by Gunasekera et al. [24] also inferred pore structure of hardened of binders in AAC affecting long-term creep property. It is understood that a high degree of polymerization results in the generation of greater volume of the hardened matrix, which fills the gaps between the unreacted FA particles and the pores to achieve

Table 1 Main chemical composition and strength of the sample [24]

Raw materials	By weight, %			BET surface area (m^2/kg)	28-day strength (MPa)	365-day strength (MPa)
	SiO_2	Al_2O_3	CaO			
Gladstone	47.87	28	3.81	2363	40.5	45.6
Pt Augusta	49.37	31.25	4.8	1229	35.6	42.3
Tarong	75.66	19	0.3	1875	20.6	42.0
PC	22.5	4.5	66.3	–	36.6	48.1

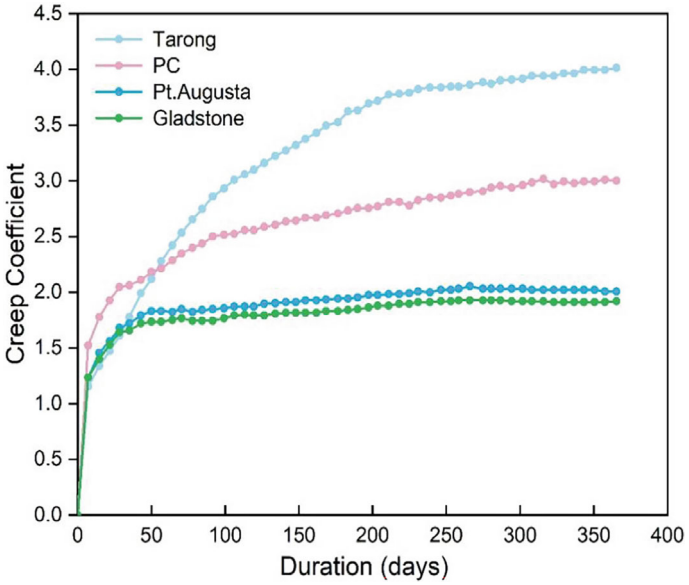

Fig. 2 Comparison between creep coefficients of FA-based AACs and PC concrete. Tarong, Gladstone, and Pt Augusta are the power stations serving as the sources of FA [24]

pore refinement. After one year of loading, the hardened geopolymer matrix in the Gladstone and Pt Augusta FA-based AACs was well-distributed, having reduced porosity in the range of 50 nm^{-1} μm, and a significant reduction in later age creep. The porosity of the Tarong FA-based AAC did not decrease significantly in the range of 50 nm^{-1} μm; the hardened matrix was less dense and filled with microcracks, resulting in significantly larger creep deformation. These results again reflect the importance of fly ash morphology and chemistry in affecting the creep property of AAC.

Blast furnace slag based AAC

GGBFS is commonly used in concrete as SCM to partially replace PC. The main advantages of using GGBFS to replace PC in the manufacture of concrete are superior durability and lower heat of hydration compared to 100% PC binders. Several studies [25–28] show that the addition of an appropriate proportion of GGBFS has an inhibitory effect on concrete creep. The mechanism of this phenomenon is attributed to the high reactivity of GGBFS itself, and the refined microstructure of concrete [26]. The reaction between silica from GGBFS and CH crystals in the hydrated PC paste produces a secondary C–S–H(II), which significantly improves the density of the paste, so the concrete creep is reduced [27, 29, 30]. However, there are discrepancies in the literature about the effect of GGBFS in creep performance. Some studies [29, 31] report that when the content of GGBFS mixed in PC concrete exceeds a certain amount, the creep of concrete is higher than that of the benchmark group. It has been

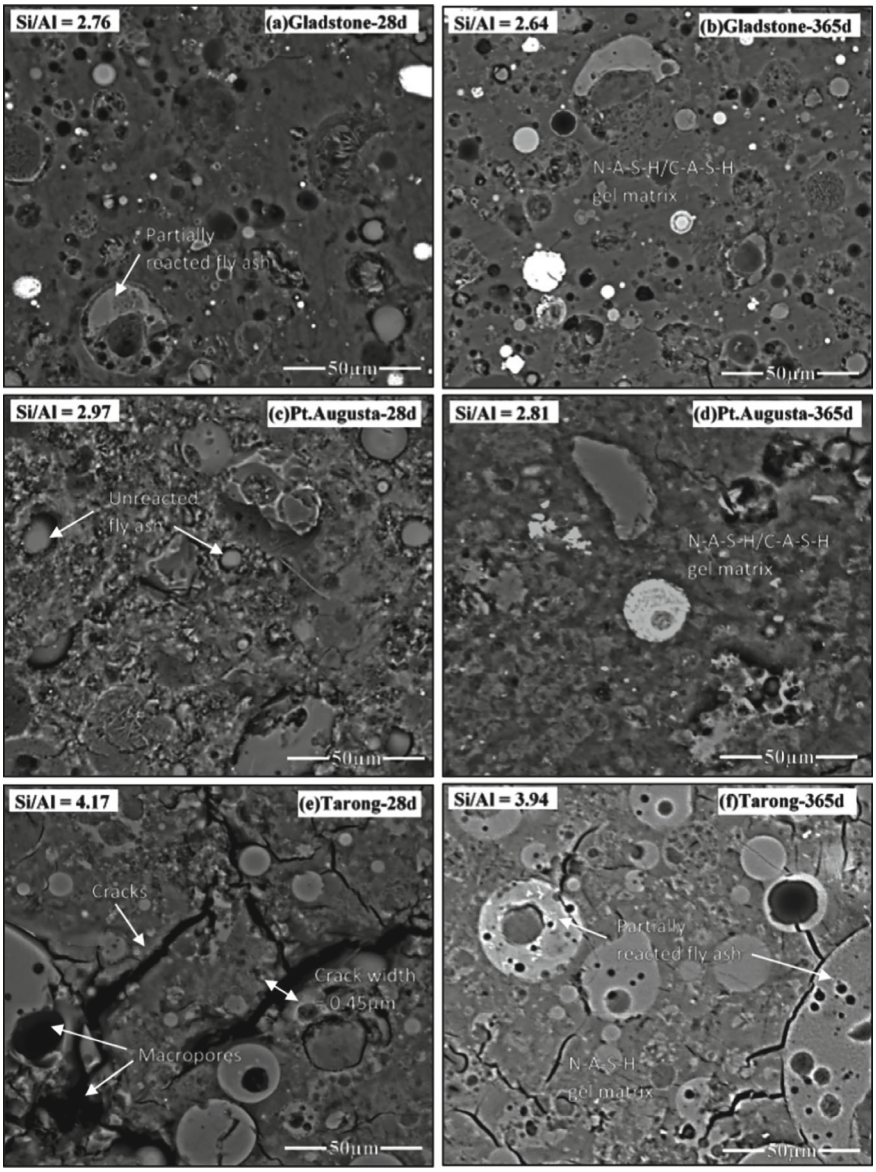

Fig. 3 Microstructural development of FA-based AACs [24]. The Si/Al shown in the figures is the apparent molar ratio of raw materials including silicate supplied from activator

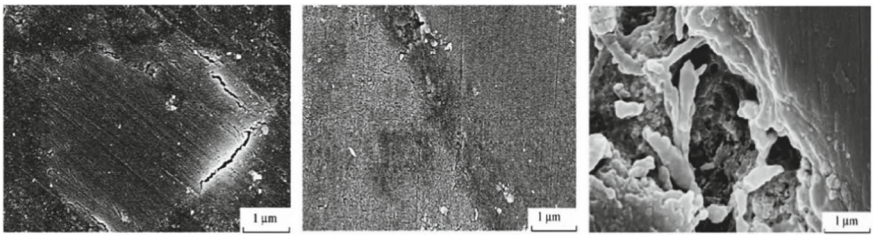

a)30% GGBFS b)50% GGBFS c)80% GGBFS

Fig. 4 SEM images of GGBFS containing PC concrete samples. Reproduced from [29]

hypothesized that this might be due to interface between the unreacted GGBFS particles and the cementitious matrix particularly at excessively high GGBFS replacement levels [19]. Micrographs shown that the concrete had a porous and loose interface between different hydration products and anhydrous GGBFS particles, which may be linked to the increased creep (Fig. 4 [29]). It must be noted, however, this is only one perspective from pore structure point of view, and the impact of slag chemistry on the hydration product composition and inherent mechanical properties cannot be ignored.

Compared with PC concrete, Collins and Sanjayan [32] studied the creep characteristics of GGBFS-based AAC. The specimens were made of dry sodium silicate activated slag, which gave enough workability and casting time. After demolding, the specimens were cured under water bath, exposure to air at 50% RH, and sealed curing in polythene bags in a sealed container, all at 23 °C. For creep testing, the specimens were bath cured for 7 days followed by 21 days of exposure curing, then subjected to load of 40% of the 28-day compressive strength. Figure 5 shows the total creep of the specimen during the loading period, where it can be observed that the creep strain of GGBFS-based AAC is higher than that of PC concrete. After 112 days, the specific creep of GGBFS-based AAC and PC concrete were 42 με/MPa and 36.7 με/MPa, respectively. It must be noted that at this specimen age, GGBFS-based AAC and PC concrete had compressive strengths of ~60 and ~50 MPa, which means the complicate relationship between creep behavior and compressive strength. Ma and Dehn [33] studied the creep characteristics of GGBFS-based AAC under different compression stress ratios.

As shown in Fig. 6, when the stress ratios are 0.50 and 0.35, the creep coefficients of GGBFS-based AAC are higher than that of PC concrete calculated by the prediction model as given by *fib* MC2010. However, there is very limited research reported with detailed explanation for this phenomenon. Humad Abeer et al. [34] evaluated the creep response of high-MgO BFS-based AAC activated by sodium carbonate, sodium silicate and their mixture. The loading was carried out at 40% of 28-day compressive strength. Their measurement showed a very large creep for all AAC specimens, which was partially associated with the small aggregate size, along with carbonation, which led to porous binder, strength loss, especially for the sodium silicate activated AAC.

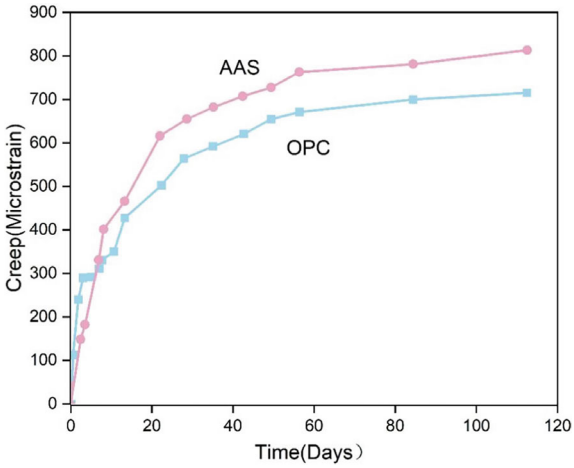

Fig. 5 Creep behaviors of PC concrete (OPC) and GGBFS-based AAC (AAS) [1]

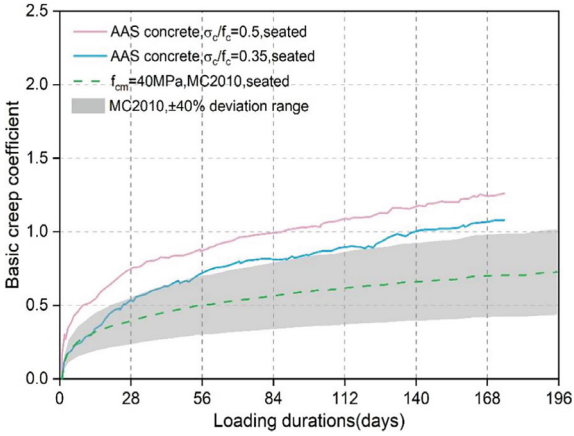

Fig. 6 Basic creep coefficient of GGBFS-based AAC [33]

Fly ash and blast furnace slag blended AAC

For PC concrete, it is possible that blending appropriate proportions FA and GGBFS can make the particle gradation of the cementitious material better. The multi-components hydrate and make the binder matrix more compact and reduce the creep [35–37]. However, for the AAC, the combined usage of FA and GGBFS as precursors cannot inhibit the creep of concrete. Hojati et al. [38] studied the long-term creep characteristics of the FA/GGBFS-based alkali-activated mortar with four different mix proportions. Table 2 shows the curing conditions and related mechanical properties of the specimens. The cylindric mortar specimens were cured under different conditions, as indicated in Table 2. After 2.5 months of moist curing, the load of 40% 28-day compressive strength was applied and continued for 20 months. The magnitude of the load was checked weekly to make sure the sustained load was not

changing over the measurement period. More details about load adjustment in the first days and weeks can been seen in [38]. Figure 7 shows the specific creep of the four different mortars. It can be observed that the specific creep increases at higher GGBFS contents, and the specific creep of the 100% FA-based alkali-activated mortar is the lowest, while the specific creep of the 100% GGBFS-based alkali-activated mortar is the highest. The compressive strength of FA-based alkali-activated mortar was the highest, and the specific creep was the lowest. On the other hand, the compressive strength of the GGBFS-based alkali-activated mortar and the mortar that contains 20% FA and 80% GGBFS are both lower and the creep is higher. It seems that there is a direct correlation between the compressive strength and the creep deformation. However, as mentioned above, the exact relationship is still a topic of research for different cases using various raw materials and manufacturing conditions.

Un [39] studied the creep properties of FA/GGBFS-based AAC with 5% FA and 95% GGBFS. Figure 8 shows the creep coefficients of the FA/GGBFS-based AAC (denoted as GPC here) and PC concrete up to 650 days of age, where it can be clearly observed that the creep behaviors of the GPC and PC concrete are different. The creep development of the PC concrete sample is fast in the first 60 days, and tends to be more stable after 150 days, and the creep increment is small. Although the creep of early GPC specimens is lower than PC concrete, the creep rate of late GPC does not decrease rapidly, and the creep trend of GPC still increases significantly after one year of loading. After 150 days, the creep of FA/GGBFS-based AAC is much higher than PC concrete, which indicates that a small amount of FA has no obvious effect on the creep characteristic of GGBFS-based AAC. A change may take place when curing conditions transfer from ambient temperature to elevated curing temperature.

The wide availability of raw materials from different sources for AAC manufacturing is advantageous from the point of view of resource efficiency, but it poses challenges for identifying general trends to draw general conclusions for the performance and service life prediction of these materials. This is particularly the case

Table 2 Curing conditions and related mechanical properties of alkali-activated mortar specimens [38]

Mixture	Curing conditions	Mortars at 28 days		Sustained stress (MPa)
		f_c (MPa)	E (GPa)	
S	Moist curing at 100% humidity and 23 °C	34.02	20.44	13.48
2F8S	Moist curing at 100% humidity	33.71	24.07	
8F2S	Moist curing at 100% humidity and 23 °C	45.94	24.21	18.37
F	Steam curing at 100% humidity and 60 °C for 1 day, and then curing at 100% humidity and 23 °C	55.78	22.74	

Note S: 100% GGBFS; 2F8S: 20% volume fraction FA, 80% volume fraction GGBFS; 8F2S: 90% volume fraction FA, 20% volume fraction GGBFS; F: 100% FA

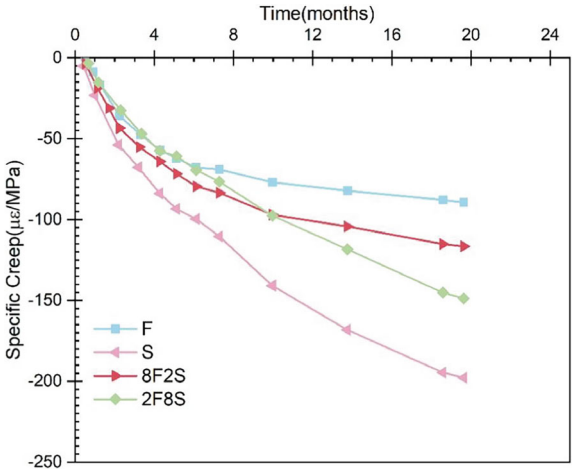

Fig. 7 Specific creep of alkali-activated mortar mixes containing different GGBFS (S) and FA (F) [38]. The mixtures and curing conditions are shown in Table 2

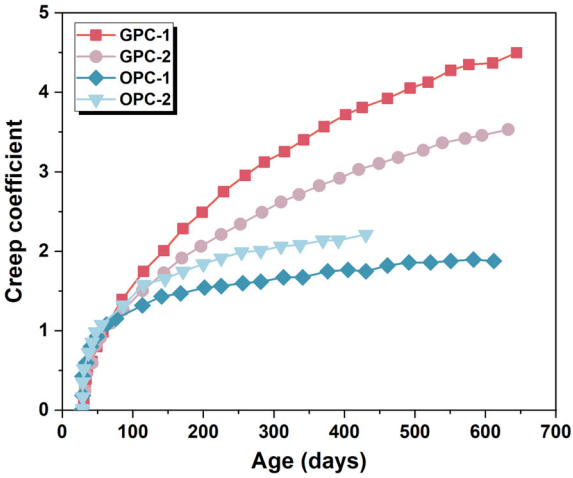

Fig. 8 Creep coefficients of FA/GGBFS-based AACs (denoted as GPC here) and OPC concrete [39]

when determining performance of structural concrete due to the limited number of studies evaluating creep deformations.

2.2 Effect of the Activator Dose

As discussed in Chap. "Conventional Precursors and Activators", in addition to the properties of the precursors used to produce AAMs, the activation conditions, comprising the activator type and amount used, also play a crucial role in the microstructure features of this materials, and consequently in their deformation and

strength developments [40–42]. Islam [43] studied the effect of activator dosage on the creep performance of low calcium FA-based AAC. The mass ratio of activator to FA varied, while a modulus of activating solution and amounts of other materials were maintained constant. The concrete specimens were cured at 60 °C for 2 days followed by curing at standard environmental conditions (50% RH and 22 ± 2 °C) and the loading method adopted was according to ASTM C512, that was 40% of the compressive strength at the testing days. Figure 9 a shows the effect of the mass ratio of activator to FA on the creep coefficient.

The creep coefficient of the sample with a mass ratio of 0.65 is 67% higher than that of the sample with a mass ratio of 0.35 during the one-year loading time. The use of more alkali activator can be considered as adding more water in the matrix; therefore, the water-binder ratio of the entire system increases. It resulted in a decrease in the compressive strength and elastic modulus of the sample, and an increase in creep [43]. This trend was also reported by Lee et al. [44], that increased water-binder ration led to more creep. It is also reported that, the creep coefficient of concrete with a compressive strength of 55.1 MPa is about 50% lower than that of 27.6 MPa after 30 days (Fig. 9b). The creep of the specimen decreases with the increase of compressive strength, which is consistent with the findings of Gunasekera et al. [24] and Wallah and Rangan [45].

2.3 Curing Conditions

Several studies have shown that curing conditions have significant impact on the creep properties of AAC. The creep deformations are closely related to the type, quantity, morphology, intrinsic strength of the reaction products and the microstructure of the hardened matrix. These properties of the paste depend on the degree of reaction, which is directly influenced by curing conditions. The temperature plays a vital role in the degree of maturity of concrete: it can accelerate the ageing process of this viscoelastic material, and as such, make them stiffer and more solid than viscous. Accordingly, moist-cured GGBFS-based AACs exhibiting creep and time-dependent deformation for a longer time than the steam-cured FA-based AAC [38]. Castel et al. [46] demonstrated the effect of temperature and humidity on the creep of FA/GGBFS-based AAC (85.2% FA and 14.8% GGBFS). Table 3 presents the curing conditions of the specimens subjected to two different rates of loading. After 8 days of curing, compressive strength and elastic modulus of the specimens by 80°C water bath curing for 7 days (i.e.7D80) were approximately twice those of the specimens by 40 °C sealed curing for 3 days (i.e. 3D40).

Figure 10 further shows the total strain and shrinkage strain (control strain) of the specimens during the 90-day loading period. The total strains of the specimens by 40 °C sealed curing for 3 days are much higher than that of the specimens by 80 °C water bath curing for 7 days. The creep strain is equal to the total strain minus the shrinkage strain. When the loading time is 90 days, the creep strain of the specimens by 40 °C sealed curing for 3 days is about 1900 με (average of 3 repeats), and the

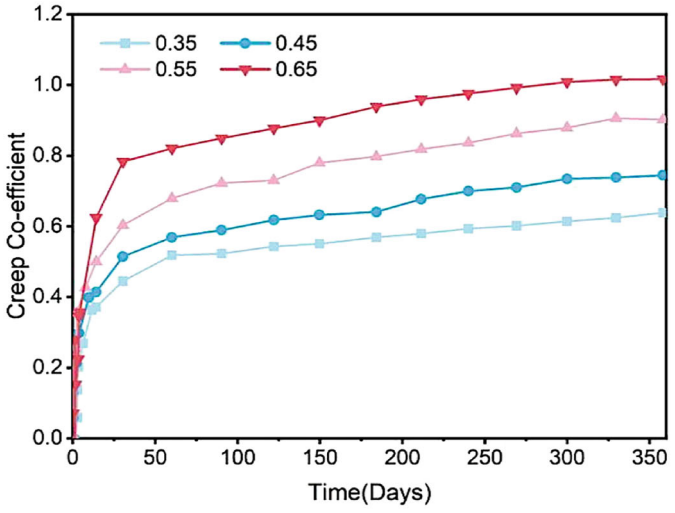

(a)

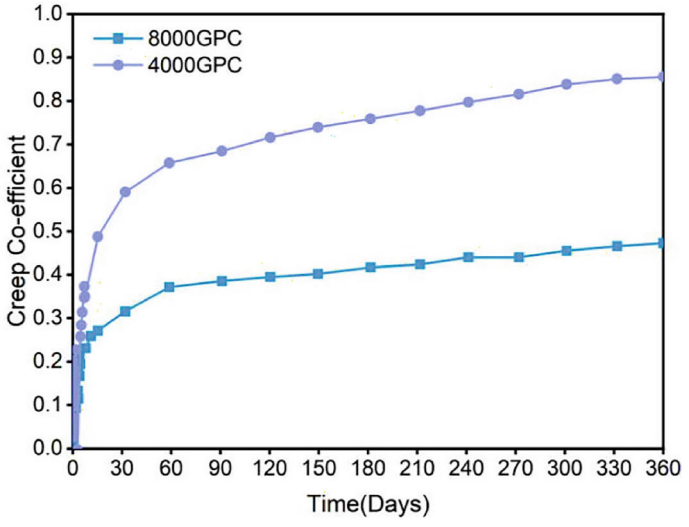

(b)

Fig. 9 Creep coefficient for FA-based AACs **a** effect of activator to FA ratio; **b** effect of strength grade (8000 GPC means 55.1 MPa concrete, while 4000 GPA means 27.6 MPa concrete) [43]

Table 3 The curing condition and loading condition of the specimen [46]

Mix ID	Age (days)	Sustained load/0.4f_c (MPa)	Average instantaneous strain (με)	Instantaneous elastic modulus (GPa)
3D40	8	10	914	10.9
7D80	8	20	911	22

Note 3D40: After casting, specimens were sealed and stored at 40 °C in an oven for 3 days and then stored in a controlled room at 23 °C and 60% relative humidity; 7D80: After casting, specimens were sealed and stored at 40 °C in an oven for 1 day and then cured in 80 °C water bath for further 7 days

creep strain of the specimen by 80 °C water bath curing for 7 days is about 200 με. This still follows the trend that the higher the compressive strength, the smaller the creep.

Although the experimental results show that water bath curing at high temperature can have a positive inhibition on creep deformations, it should be noted that it is not necessary that water bath gives higher compressive strength than steam or air curing at the same temperature. Wei et al. [47] studied the microstructure of blended fly ash sinking beads/GGBFS-based AAM after water bath curing and standard curing. The paste specimens were prepared using sodium silicate and sodium carbonate as activator at a dose of 10% in the total solid materials (including the fly ash sinking beads and GGBFS and dry activator, this was referred as one-part binder). After mixing at water to binder ration of 0.35, the specimens were cured for 24 h at

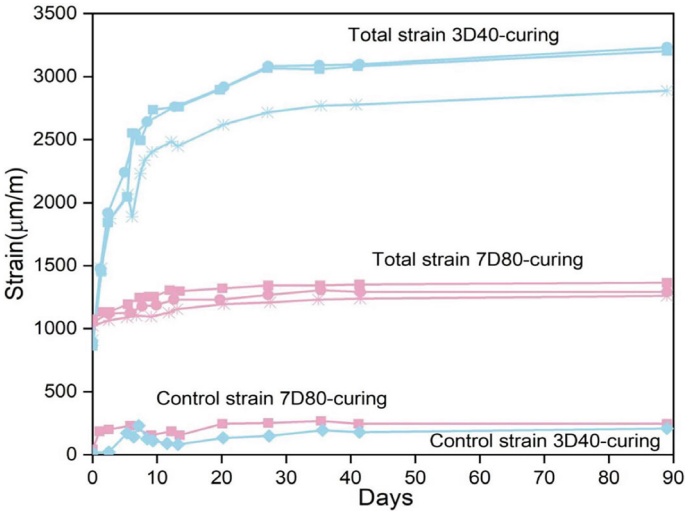

Fig. 10 Total strain and control strain of FA/GGBFS-based AACs (specimens were not loaded under the same conditions). Reproduced from [46]

standard room conditions, demolded, followed by curing at two different conditions: standard curing at 20 ± 2 °C, 95 ± 3% RH in a sealed bag; water bath curing in a water tank at 20 ± 2 °C. After 28 days of water curing, in a scope of 75 mm × 45 mm, microcracks with a width of several micrometers and a length of several tens of micrometers were also detected in the samples. Athira et al. [48] showed that water bath curing reduces the compressive strength of the samples due to the leaching of the alkaline solution into the surrounding water, and the decrease in the activator concentration leads to a decrease in the compressive strength [49]. Another study also pointed to a similar explanation that the leaching of activator ions would affect the reaction of FA, and thus the water bath-cured AAMs would form a porous microstructure [50]. Therefore, for the determination and comparison of creep results among different AAMs, curing conditions must be accounted for.

It is well known that the curing conditions applied to AACs affect the microstructure features of the materials, and consequently the mechanical properties, including creep. Xie et al. [37], Lin et al. [51], Wang et al. [52] and Peng et al. [53] studied the effect of curing temperature on the strength development of FA-based AAC, carbonate mineral alkali-activated paste and metakaolin alkali-activated paste, respectively. The results showed that in a temperature range from 20 to 100 °C, with the increase of curing temperature, the compressive strength first increased and then decreased, and the temperature for achieving the peak compressive strength of samples with different raw materials was different. Conversely in a temperature range from 20 to 60 °C, the compressive strength of all three AAM systems evaluated increased. Häkkinen [54] identified that for the GGBFS-based AAC, the thermal curing at 70–80 °C can be detrimental. It may cause AAC to lose too much water during reaction, leading to cracking and shrinkage. Although high temperature accelerates the activation reaction, resulting in a denser structure, when the temperature is too high (>60 °C), the rapid loss of water usually causes thermal damage and cracks in the specimen.

Wallah and Rangan [45] studied the creep properties of FA-based AACs under two conditions: dry curing and steam curing. The curing conditions and loading conditions of the specimens are shown in Table 4. It should be noted that all the specimens were subjected to 60 °C curing for 1 day at both dry and steam conditions. From the data in the table, it can be seen that the compressive strength of the steam curing specimens is about 15% lower than the dry curing specimens, and the elastic modulus is about 8% lower than that of the dry curing specimens.

Figure 11 shows the specific creep of the specimens loaded for one year, and at the same mix ratio, the specific creep value of the steam-cured specimens is higher.

Overall, the final specific creep value of FA-based AAC after one year of loading is inversely proportional to the compressive strength. The higher the compressive strength of the specimen, the lower the specific creep value, which is consistent with the conclusion found earlier. The results showed that the use of steam curing reduces the strength of the concrete and increases the creep variable [45]. Analysis of the microstructural differences causing the variations in performance were not investigated in this study, which deserves further investigation.

Table 4 Mix compositions, curing conditions and loading conditions of FA-based AAC. Data from [45]

Mix	Modulus of alkali activator ($nSiO_2/Na_2O$)	Water-solid ratio	Curing conditions	Sustained stress/$0.4f_{c7}$ (MPa)	Instantaneous Elastic Modulus (GPa)
1CR	0.74	0.2	Dry	27	29.6
2CR	0.74	0.2	Steam	23	26.9
3CR	0.88	0.23	Dry	19	22.9
4CR	0.88	0.23	Steam	16	21.1

Notes Water is mass of the added water plus the water contained in activator solution; solid is the mass solids contained in activator solution and the mass of FA; **Dry**: oven curing at 60 °C for 1d, followed by room temperature curing for 6 d; **Steam**: steam curing at 60 °C for 1d, followed by room temperature curing for 6 d

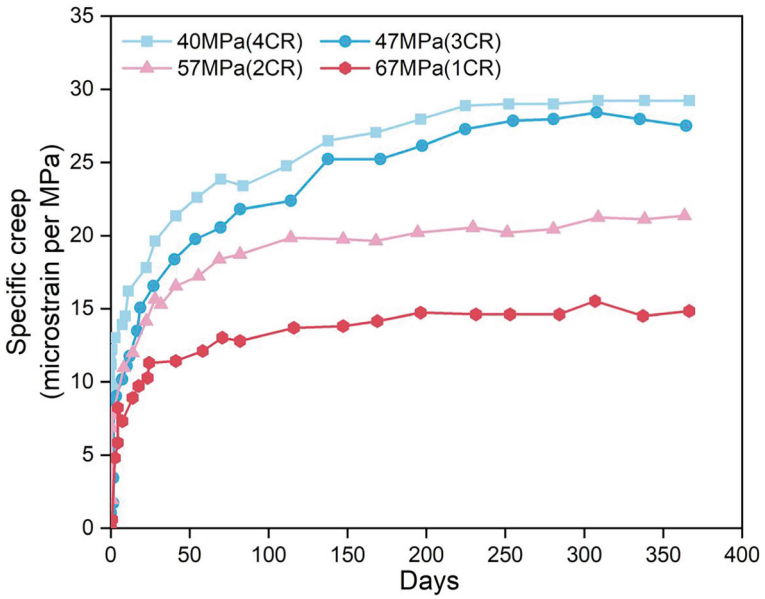

Fig. 11 Effect of curing conditions and resultant compressive strength on creep of AAC [45]. Specimens 2CR and 4CR are subjected to steam curing at 60 °C for 1 day, while 1CR and 3CR are subjected to dry curing at 60 °C for 1 day, then all followed by room temperature curing for 6 d

Gunasekera et al. [24] and Sagoe-Crentsil et al. [21] studied the creep properties of two low-calcium FA-based AAC, respectively. The chemical composition and curing conditions of the two FA are shown in Table 5.

The measured specific creep and strain of Type 1 FA-based AAC are similar to those of PC concretes of the same strength grade. The creep coefficient of Type-2 FA-based AAC at 365 d is about 40% of that of PC concrete. The raw materials and

Table 5 Summary of the two FA types and the curing conditions of AAC adopted in different studies to evaluate deformation performance

FA type	By weight, %			Curing conditions	Creep	References
	SiO_2	Al_2O_3	CaO			
Type-1	47.87	28	3.81	Room temperature curing for 1 d, 80 °C oven curing for 1 d	High	[24]
Type-2	47.19	29.79	3.29	Steam curing at 65 °C for 6 h	Low	[21]

mix proportions of the two concretes are similar, and it can be concluded from the above research that steam curing will increase the creep of the specimen, however, temperature should play an even more important role governing creep than humidity in curing.

2.4 Incorporation of Fibers

Banthia and Gupta [55] showed that polypropylene (PP) fiber has the potential to reduce the creep and shrinkage of PC concrete, which has been proven in many subsequent studies. However, differences in the chemistry and microstructure of AAC compared to PC concrete result in considerable different adhesion properties between the fibers and the matrix, and therefore, fibers in an AAM matrix may not necessarily have the same properties/functions as fibers in PC.

Noushini et al. [56] evaluated AAC that prepared with 85% FA and 15% GGBFS as raw materials, mixed with 0.5% PP fiber and studied its effect on the creep properties. The specimens were cured at 75 °C for 18 h, and the creep test was started after curing for 28 d at temperature of 23 ± 2 °C and relative humidity of 50 ± 5%. As shown in Table 6, since the elastic modulus of PP fibers is lower than that of the concrete matrix, the elastic modulus of the fiber-incorporated composites decreases. The compressive strength of all fiber-reinforced AACs was lower than that of the control specimens, which may be due to the fact that the incorporation of fibers introduced small internal pores and weak interface in the matrix of AAMs.

Figure 12 shows the creep coefficients of the fiber-reinforced AACs: the addition of synthetic fiber increases the creep of FA-based AAC. The creep coefficients increase by 19% after adding PP fiber, and the creep coefficients of AAC increases by 30% after adding PO fiber. The incorporation of organic fibers seems to cause internal defects and lower modulus, leading to increase of creep deformation. Zhao et al. [57] comparatively studied the creep of PC concretes mixed with steel fiber, polyvinyl alcohol (PVA) fiber, PP fiber and basalt fiber. After loading for one year, the test of concretes that had 28-day compressive strengths in a range of 35.3

Table 6 Elastic modulus and loading conditions of AAM concrete at age 28 d [56]

Mix	Modulus of elasticity (GPa)	28-days cylinder compressive strength (MPa)	Sustained load (%)	Sustained load (MPa)
GPC-P	28.8	50.4	40	20.2
GPC-PP18	26.3	46.7	40	18.7
GPC-PP19	27.5	46.7	40	18.7
GPC-PP51	24.3	47.3	40	18.9
GPC-PO48	25.6	43.8	40	17.5
GPC-PO55	24.6	43.6	40	17.4

Note Mix name: GPC means low-calcium FA-based AAC. P, PP and PO represent plain (without fiber), polypropylene fiber and polyolefin fiber, respectively. The following number, i.e. 18, 19 etc. means the length of fibers

and 38.0 MPa showed that when the PVA and PP fibers were introduced, specific creep was increased; when steel fiber and basalt fiber were used, specific creep was increased. The authors [57] pointed out that elastic modulus of fiber was critical to the creep resistance of concrete. Although lower fiber elastic modulus dissipates energy and improves ductility due to its high deformability, it does not improve long-term deformation of concrete at low stress levels.

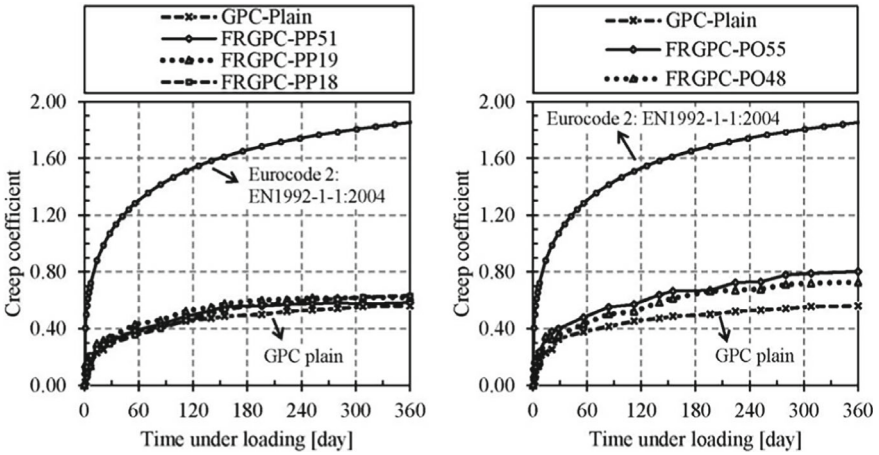

Fig. 12 Creep coefficient of plain and fiber-reinforced AAC [56] (The meaning of each mixture and the loading conditions can be seen in Table 6)

2.5 Loading Conditions

Concrete creep is dependent on a number of experimental factors, including loading type (compressive or tensile), loading level, environmental temperature and relative humidity. In the above summarised cases that reported in literature all have specified environmental temperature and relative humidity when loading is performed.

The significant contribution of both tensile and compressive sustained stress to creep deformation of concrete is generally recognized. However, not so many studies on long-term tensile creep are available in the literature due to technical difficulty of such tests [58–60]. Temperature stress testing machine (TSTM) is one of the rare methods enable to perform tensile and compressive creep tests under nominally identical conditions, e.g. dimensions, curing conditions, measurement set-up and load-regime. Li et al. [61] demonstrated the influence of creep and relaxation on the cracking potential of the FA/GGBFS blended AAC using TSTM. Klausen et al. [62] used the TSTM to perform test series and found that PC concrete with FA obtained similar creep behaviors in compression and in tension. However, no experimental results are reported yet on the comparison between tensile and compressive creep of AAC.

In literature, so far, most of the research on AAC creep were in compression model, as shown in the above sections, and very limited information has been reported about tensile creep. Tensile creep will relax the tensile stress, if the tensile creep is ignored, the tensile stress inside the concrete will be overestimated and the service performance of the structure will be underestimated. Cheng et al. [63] evaluated low-calcium FA activated with a mixture of sodium hydroxide and sodium silicate solution as alkaline activator, determining the early ageing coefficient of AAC experimentally. It musted noted that 10% GGBFS was used to accelerate setting, and the water to binder ratio was 0.345. After curing at 80 °C for 24 h, the dog-bone AAC specimens were subjected to continuous tensile loading at 2, 3, 4, 7, 14 and 21 days respectively (the continuous tensile stress was 50% of the tensile strength of the corresponding age member), and the ageing coefficient of tensile creep of AAC was calculated by stepwise numerical analysis. Figure 13 shows the calculation results of average tensile creep coefficient of AAC. In the creep coefficient vs. time curves, AAC shows typical ageing effect: the tensile creep coefficient decreases with the increase of the first loading time τ_0. The ageing effect of AAC should be fully considered in the analysis of tensile creep effect.

Figure 14 shows the calculated tensile ageing coefficient of the AAC evaluated in [63]. Tensile creep reduces constrained shrinkage strain and reduces potential tensile stress and cracking risk. As the ageing coefficient decreases, the crack risk analysis becomes more conservative. Therefore, in structural design, it was recommended that the ageing coefficient of the high temperature cured AAC in the early stage (2–28 days) can be approximately set as 0.8 [63]. To verify this, in the same study [63], the authors used the ageing coefficient to analyze the risk of early cracking of FA-based AACs. The results show that the mean value and variance coefficient of calculated stress and measured stress ratio before cracking of concrete ring are 0.98

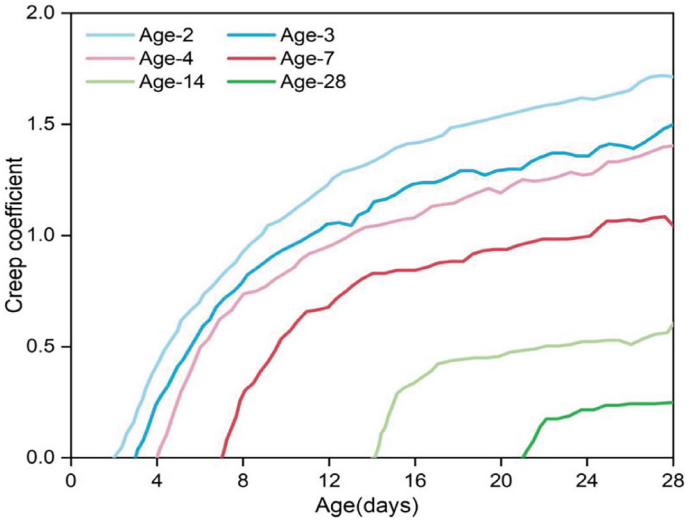

Fig. 13 Average creep coefficient of the tested FA-based AAC specimens initially loaded at $\tau_0 =$ 2, 3,4, 7, 14, 21 days respectively. Reproduced from [63]

and 0.02, respectively. This indicates that the proposed ageing coefficient of 0.8 can be used to analyze the risk of early cracking of FA-based AACs.

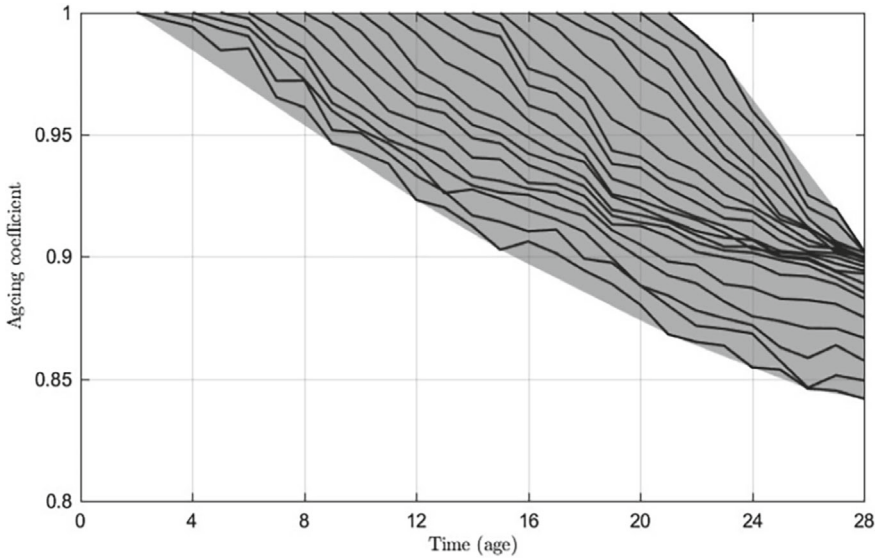

Fig. 14 Calculated ageing coefficient for AAC subjected to sustained tension at early age. Reproduced from [63]

Given the importance of ageing effect, loading time is therefore crucial for creep testing. In a study of the applicability of existing creep prediction equations of PC concrete to AAC by Un [39] (which will be further discussed later), the author showed the difference caused by loading time. The AAC were prepared with 95% GGBFS and 5% FA using sodium silicate as an activation solution at 0.4 liquid-to-binder ratio. The creep was tested on two reinforced 600 mm × 240 mm × 6500 mm beams. The 28-day compressive strength and flexural strength of concrete samples subjected to the standard bath curing were reported to be of 46.7 MPa and 6.8 MPa respectively. An PC concrete sample of the same strength grade demonstrated flexural strength was 4.1 MPa. On top of the beams at the age of 14 days self-weight and sustained load of 1 kPa were applied to simulate construction conditions. With respect to the long-term variation of the creep coefficient of samples loaded after 14 and 28 days of curing (Fig. 15), the author highlighted the lasting (1 year) downgrade in creep strains in the case of the early load application (14 days).

Loading level is another critical factor that affects creep performance. The study by Zhou et al. [64] compared creep of GGBFS-based AAC under a stress–strength ratios from 0.15 up to 0.75. Within that range, the creep of AAC has a convergent nonlinear stage and a non-convergent stage but not an obvious linear stage. This phenomenon differs from that in PC concrete, which has typically linear creep stage under a stress–strength ratio of 0.4. The dividing points of the convergent nonlinear creep and non-convergent creep of GGBFS-based AAC are above 0.6 and approximately 0.75, which are quite similar with those of PC concrete. The GGBFS-based AAC

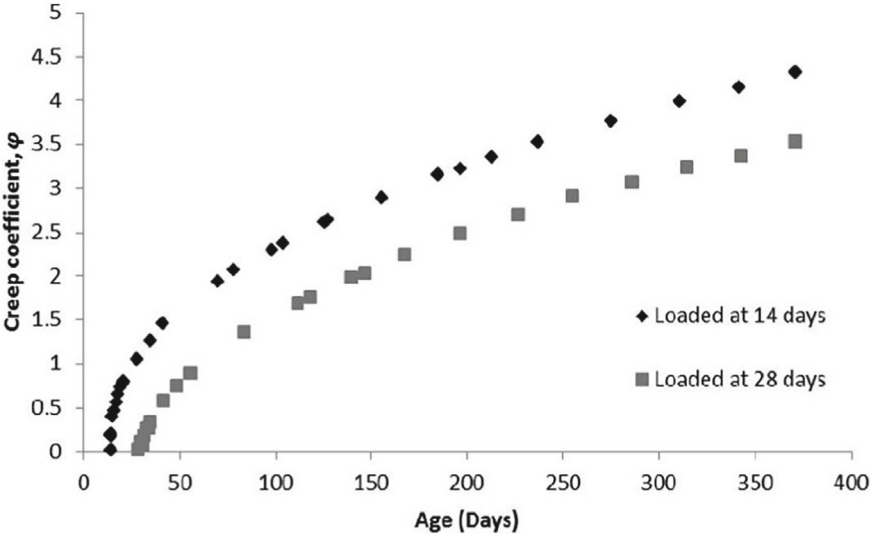

Fig. 15 Long-term evolution of the AAC beam creep coefficient when loaded at 14 and at 28 days. Reproduced from [39]

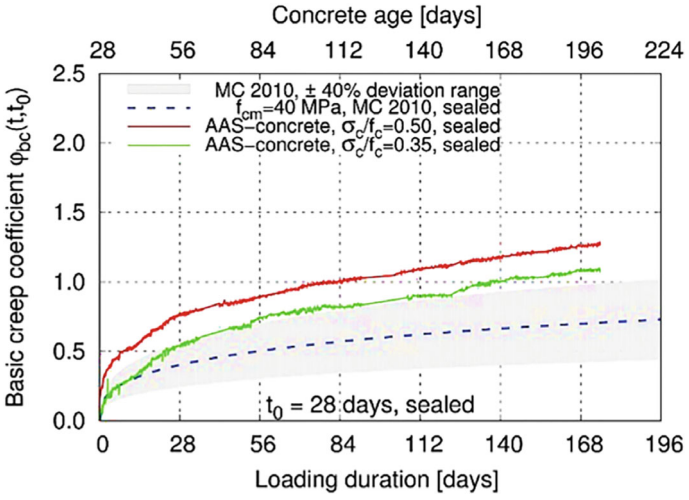

Fig. 16 Effect of loading and humidity on creep coefficient of GGBFS-based AAC [33]

basically has a consistent creep coefficient under a stress–strength ratio of 0.15–0.6 and provides a convenient way to achieve a creep prediction. Ma and Dehn [33] also investigated the creep in GGBFS-based AAC with different stress–strength ratios (0.35 and 0.5) but under two different conditions of relative humidity (65% and sealed) for approximately 180 days. The researchers compared the test results with the results from creep model of CEB-FIP 2010 [52], and found that the experimentally determined creep coefficient of GGBFS-based AAC is higher than predicted (see Fig. 16).

3 Creep Mechanisms

The creep mechanisms in PC concrete have been investigated for many decades. The complete explanation is not formulated yet. However, substantial progress has been made in this area. Bažant in his monograph [6] summarized several theories describing the mechanisms causing and influencing creep: plastic flow, consolidation theory, loading bearing hindered adsorbed water, bond breakage in slip and its reformation, nonlinear deformations and cracking as a contribution to Pickett effect (drying creep), solidification theory for short-term ageing, microprestress of creep sites in cement gel microstructure and its relaxation [65]. These mechanisms most probably are also present in the AAC as well, although the specific microstructure and mechanical properties may lead to different specific features of creep. Un [39] discussed that the sustained loading results on GGBSG/FA-based AAC in more slippage of phases, and alternation of microstructure to denser phases, which further results in larger creep deformation. Moreover, migration of water in the pore network

causes non-negligible drying creep. AAC is usually more sensitive to temperature than PC concrete due to the increasing visco-flow behaviour and further reaction subjected to high temperature.

For GGBFS-based AAC, evident viscous deformation of alkali-activated GGBFS is due to the rearrangement of C–A–S–H matrix [66]. The reason for the greater viscoelasticity of the C–A–S–H matrix compared to C–S–H is the structural incorporation of alkali cations in C–A–S–H. It reduces the stacking regularity of C–A–S–H layers and makes the matrix easier to collapse and redistribute [66]. The large creep of alkali-activated GGBFS systems contributes also to their large shrinkage (either autogenous or drying), which consists of not only elastic but non-elastic deformations [67, 68]. With the experimentally measured relative humidity of the paste, elastic modulus and saturation degree as inputs, Li et al. [67] calculated the elastic deformation of alkali-activated GGBFS paste under capillary pressure and found that it accounts for only less than 25% of the total autogenous shrinkage. Very similar proportions of elastic deformation were identified by Abate et al. [68]. These studies proved that non-elastic deformation needs be considered in predicting the autogenous shrinkage of GGBFS-based AAC.

Based on the understanding of creep contributor, Li et al. [67] used an empirical equation to calculate the creep coefficient based on degree of reaction and w/b ratio, and accumulated the increments of creep formed in each time interval (Fig. 17). Alternatively, Abate et al. [68] applied a spring-dashpot model to simulate the creep compliance of GGBFS alkali-activated paste (Fig. 18). Both these approaches result in good predictions of the autogenous shrinkage of GGBFS alkali-activated pastes, indicating that these models approach the real mechanism of creep happened in alkali-activated GGBFS systems.

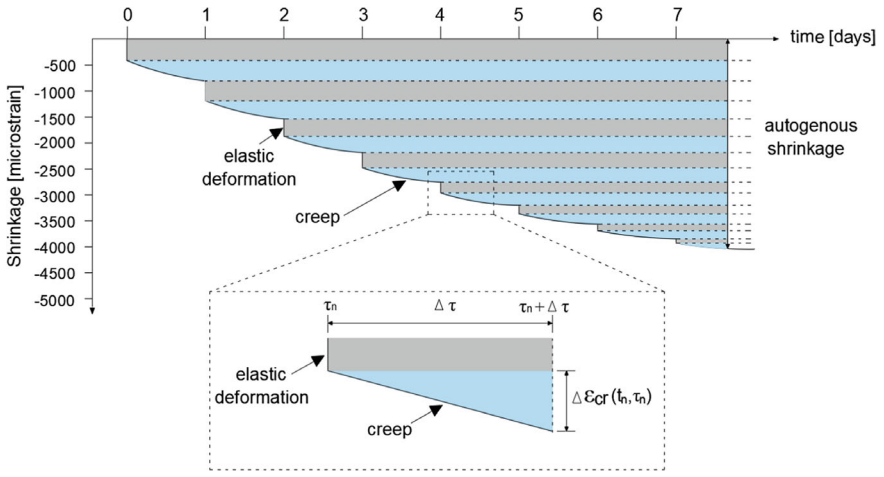

Fig. 17 Schematic representation of the model used to simulate the creep mechanism over time of GGBFS alkali-activated paste. Reproduced from [67]

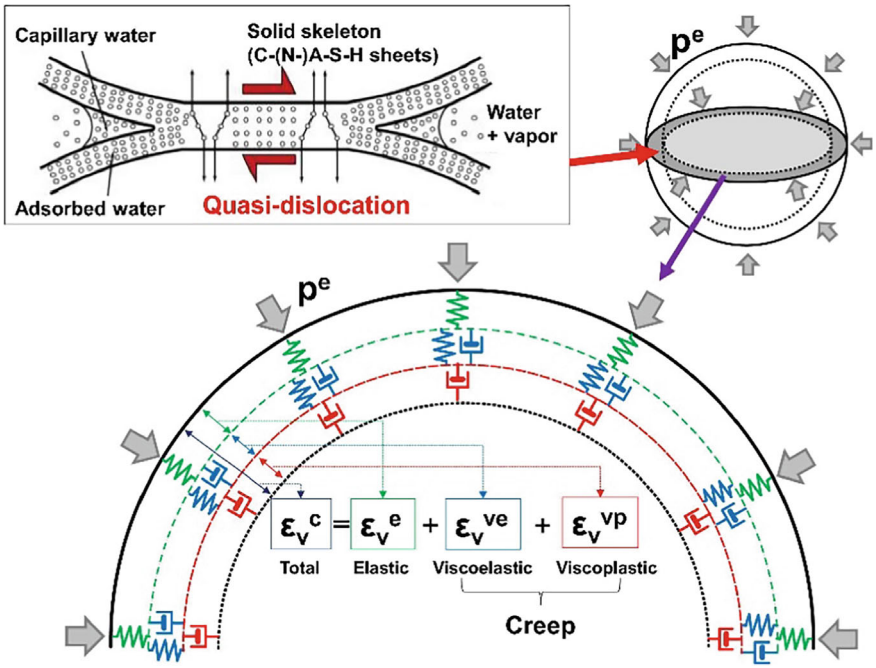

Fig. 18 Schematic representation of equal mechanical components to simulate the creep compliance of alkali-activated GGBFS paste. Reproduced from [68]

4 Creep Models for AAC

In engineering practice, the creep prediction model given by the specification is often directly selected, and an existing model is usually modified according to a small amount of test data, so as to calculate the long-term ageing characteristics of concrete creep [69]. Compared with the PC hydration reaction, the hydration and polymerization reactions of AAMs are more complex and have more influence factors on creep. Therefore, it is necessary to explore the creep prediction models of AAC to be extended and applied to practice [70, 71].

Castel et al. [46] compared the measured creep coefficients of a GGBSF/FA blended AAC after curing under different conditions with the creep coefficients predicted using the EN1992-1-1:2004 model [72], and the results are shown in Fig. 19. The actual creep coefficient of the 7D80 specimen (the meaning of denotes refer to the note of Table 3) is about 90% lower than the coefficient predicted by the model, while the actual creep coefficient of the 3D40 specimen is close to the coefficient predicted by the model before 45 days, since when the prediction results are much higher. Experiments showed that changes in curing conditions will greatly affect the prediction accuracy of the model. From this study, it suggests that the EN1992-1-1:2004 creep prediction model generally overestimates the creep of the

GGBSF/FA-based AAC from a long-term view and cannot be applied to the creep prediction directly.

Hojati et al. [38] compared the creep test data of an alkali-activated FA/GGBFS blended mortar with the predicted value of the ACI-209R model. The detailed sample preparation and creep testing conditions are given in Fig. 10. The comparison result is given in Fig. 20, which shows a large difference.

Hojati et al. [38] adapted the ACI-209R model by modifying the traditional creep coefficient expression from (Eq. 1) to (Eq. 2) and obtained the independent variables by applying nonlinear least squares estimation. The regression analysis results are shown in Fig. 21. The coefficient of determination R^2 for any experimental group predicted by the revised model is above 96.24%.

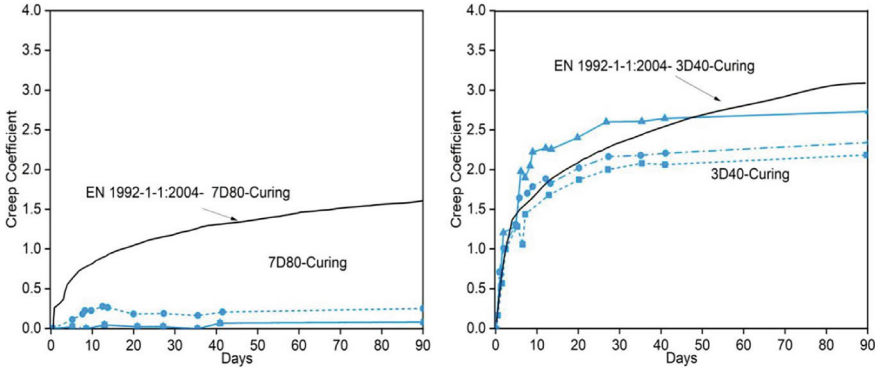

Fig. 19 Creep coefficients experimentally measured and predicted by model of EN 1992-1-1:2004. Reproduced from [46]

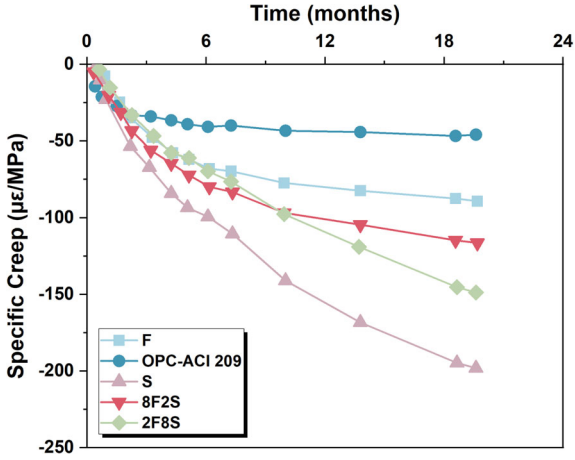

Fig. 20 Specific creep of alkali-activated FA/GGBFS blended mortar and PC mortar (according to ACI-209 model). Reproduced from [38]

$$\varphi(t, t_0) = \frac{(t - t_0)^{0.6}}{10 + (t - t_0)^{0.6}} \varphi(\infty, t_0) \tag{1}$$

$$\varphi(t, t_0) = \frac{(t - t_0)^{A}}{B + (t - t_0)^{C}} D \tag{2}$$

Un [39] studied the creep of GGBFS/FA-based AAC (5% FA and 95% GGBFS) and compared it with several existing creep prediction models. As shown in Fig. 22, none of the creep models precisely predicted the creep curves of the AAC specimens over the approximately 1-year test period. Although the predicted and actual values of the AS3600-2009 model are the closest, the creep curve overestimates the early creep effect and underestimates the late creep effect.

Un [39] adjusted all creep prediction models, and the final fit showed that the adjusted ACI model had the highest applicability and accuracy. The modified model parameters are shown in Table 7. Concrete strength correction coefficient is introduced, and other influencing factors are the same as PC concrete, but the selection of specific parameters is different. Figure 23 shows the comparison of the predicted data of the revised ACI model with the experimental data, and the results show that the revised model produces accurate creep predictions for all test specimens.

Wallah and Rangan [45, 73] reported an example of using a prediction method that was developed by Gilbert [74] for PC concrete to predict the creep and shrinkage of

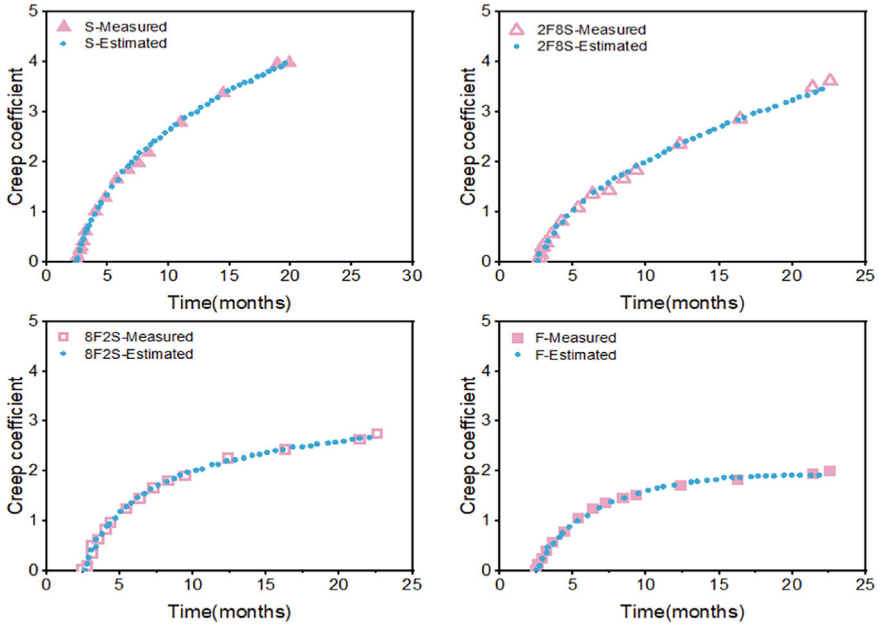

Fig. 21 Fitting curve of creep coefficient vs. time and sets of observation points for different AAMs. Reproduced from [38]

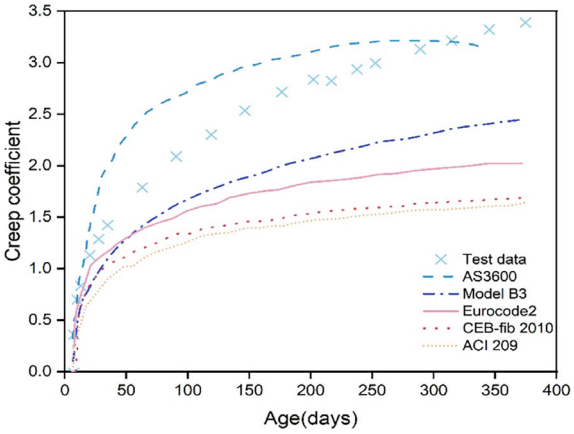

Fig. 22 Prediction of creep coefficient with standard creep models. Reproduced from [39]

Table 7 AAC creep model based on ACI model [39]

Model components	GPC-ACI	ACI
Creep coefficient	$\varphi_t = \frac{t^{\omega}}{10+t^{\lambda}}\varphi_u$	$\varphi_t = \frac{t^{\psi}}{d+t^{\psi}}\varphi_u$
Ultimate creep coefficient, φ_u	$\varphi_u = 2.35\gamma_c$ $\gamma_c = \gamma_{fcm}\gamma_{la}\gamma_{\lambda}\gamma_h\gamma_s\gamma_{\psi}$	$\varphi_u = 2.35\gamma_c$ $\gamma_c = \gamma_{la}\gamma_{\lambda}\gamma_h\gamma_s\gamma_{\psi}$
Age of loading factor, γ_{la}	$\gamma_{la} = 1.6{t_{la}}^{-0.2}$ For moist cured concrete	$\gamma_{la} = 1.25{t_{la}}^{-0.118}$ For moist cured concrete
Relative humidity factor, γ_{λ}	$\gamma_{\lambda} = 1.27 - 0.006RH$	$\gamma_{\lambda} = 1.27 - 0.67RH$ For RH > 40%
Strength of concrete factor, γ_{fcm}	$\gamma_{fcm} = 40{f_{cm}}^{-1.5}$	None

Note GPC means AAC

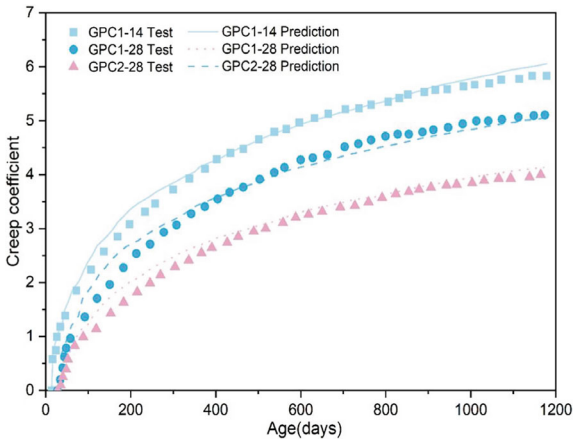

Fig. 23 Prediction of creep coefficient on AAC using modified ACI model. Reproduction from [39]. GPC1-14 and GPC1-28 means GGBFS/FA-based loaded at 14 days and 28 days, respectively (GPC2-28 means GGBFS/FA-based AAC from another batch loaded at 28 days)

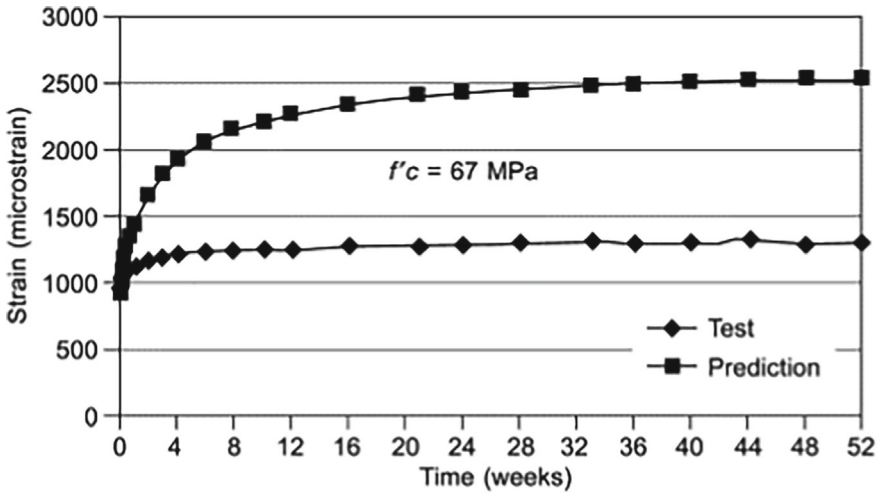

Fig. 24 Correlation of test and predicted creep strain data according to Wallah and Rangan [45]

FA-based AAC. The comparison of the experimental results with the values calculated by Gilbert's method is shown in Fig. 24. It shows that the measured creep strain of FA-based AAC is significantly smaller than the predicted values. As it was discussed in Sect. 1.1, the creep strains FA-based AAC are smaller than that of PC concrete and the method of prediction confirms that fact too. It is obvious that a new prediction method is required which could provide a more accurate prediction of the properties for FA-based AAC.

At present, the research progress of AAC creep is still very limited. The creep prediction model of AACs has not been really launched. It is found that the existing creep prediction models for PC concrete is generally unsuitable for AAC, and an ideal prediction accuracy may be achieved after proper parameter correction, as demonstrated by the work by Un [39]. There are many similarities in the factors affecting the creep of AAC and PC concrete, but the sensitivity of AAC to these influencing factors is different from that of PC concrete. In the future, substantial work is needed to study creep of AAC from different type of raw materials. The relationship between creep and composition and manufacturing conditions should be clarified and built up for the construction design purpose.

5 Concluding Remarks

In the past 30 years, limited research has been conducted on the creep behavior of AAC where the potential effects of material compositions, manufacturing processes and loading conditions have been assessed. The testing conditions adopted as well as the materials evaluated are very different from each other which poses a challenge

to identify generalized trends about the behaviour of AAC. Nevertheless, there is a general consensus that AAC produced with FA, GGBFS or their blends present vibrable creep behaviors. However, the limited studies in the topic highlight that existing creep prediction models for PC concrete cannot be directly transferred and adopted to AAC.

For the same strength grade, the creep of thermally cured FA-based AAC is normally lower than PC concrete, and the creep of GGBFS-based AAC is comparable or higher than PC concrete. This means the reaction products, i.e. zeolitic semi-crystalline N–A–S–H in thermally cured FA-based alkali-activated and highly amorphous C–A–S–H in room temperature cured GGBFS-based alkali-activated binders, behave differently under a constant loading. In addition, the pores between 50 nm-1μm and porosity are found to have significant impacts on the creep characteristics.

Cautions must be paid to curing conditions before creep testing. For most GGBFS-based AAC, room temperature curing is widely used as the strength development is quick enough. For FA-based AAC and blended AAC with much high content of FA that need thermal curing, the changes of microstructure development due to temperature varying must be considered. A temperature above 80 °C cause thermal defects and cracks in hardened concrete, which greatly increases the creep. The water bath curing method, in fact not recommended, is suitable only for AAC with high concentration of alkali activator. Direct immersion will lead to diffusion of alkalis into water, thus an insufficient reaction and a loose internal structure and increased creep. For most FA-based AACs, the recommended curing method is to use thermal curing at about 60 °C. Curing time and initial loading time are also important in testing.

Considering the outcomes of the current review, more creep research on both small size and full-scale size AAC test samples is needed. Since the creep mechanism of AAC is different from that of PC concrete, using the creep prediction model of PC concrete will produce large error in practice. New models based on different types of raw materials and different manufacturing conditions are needed, which leaves a much large research gap.

Acknowledgements The authors wish to express their gratitude to the RILEM Technical Committee 294-MPA (Mechanical Properties of Alkali-Activated Materials) for offering the platform to conduct this review and gain valuable insights into alkali-activated concrete (AAC). The authors also extend their appreciation to their respective institutions and organizations for providing the necessary resources and support to prepare this chapter. Special thanks are due to Yongchao Guo, Jie Hu for their contribution to collection relevant literature and discussion. The writing corrections and suggestions from Jelle Bezemer are acknowledged.

Authors' Contributions All authors contributed to this paper. All authors read and approved the final manuscript.

Conflicts of Interest The authors declare no conflict of interest.

References

1. Alexander, M., Bentur, A., Mindess, S.: Durability of Concrete: design and Construction, 1st edn. CRC Press, Boca Raton (2017)
2. Bernal, S.A., Provis, J.L.: Durability of alkali-activated materials: progress and perspectives. J. Am. Ceram. Soc. **97**(4), 997–1008 (2014). https://doi.org/10.1111/jace.12831
3. Arbi, K., Nedeljković, M., Zuo, Y., Ye, G.: A review on the durability of alkali-activated fly ash/slag systems: advances, issues, and perspectives. Ind. Eng. Chem. Res. **55**(19), 5439–5453 (2016). https://doi.org/10.1021/acs.iecr.6b00559
4. Bao, J., Wang, Y., Zhang, H., Li, S., Zhang, P., Qin, L., Song, Q.: Effect of loading-induced damage on chloride ingress behavior of recycled aggregate concrete: a comprehensive review. Cem. Concr. Compos. **141**, 105123 (2023). https://doi.org/10.1016/j.cemconcomp.2023.105123
5. Castel, A., François, R., Arliguie, G.: Effect of loading on carbonation penetration in reinforced concrete elements. Cem. Concr. Res. **29**(4), 561–565 (1999). https://doi.org/10.1016/S0008-8846(99)00017-4
6. Bažant, Z.P.: Prediction of concrete creep and shrinkage: past, present and future. Nucl. Eng. Des. **203**(1), 27–38 (2001). https://doi.org/10.1016/S0029-5493(00)00299-5
7. Li, K., Li, L.: Crack-altered durability properties and performance of structural concretes. Cem. Concr. Res. **124**, 105811 (2019). https://doi.org/10.1016/j.cemconres.2019.105811
8. Sousa, H., Bento, J., Figueiras, J.: Construction assessment and long-term prediction of prestressed concrete bridges based on monitoring data. Eng. Struct. **52**, 26–37 (2013). https://doi.org/10.1016/j.engstruct.2013.02.003
9. Kai, M.F., Zhang, L.W., Liew, K.M.: New insights into creep characteristics of calcium silicate hydrates at molecular level. Cem. Concr. Res. **142**, 106366 (2021). https://doi.org/10.1016/j.cemconres.2021.106366
10. Pardal, X., Brunet, F., Charpentier, T., Pochard, I., Nonat, A.: ^{27}Al and ^{29}Si solid-state NMR characterization of calcium-aluminosilicate-hydrate. Inorg. Chem. **51**(3), 1827–1836 (2012). https://doi.org/10.1021/ic202124x
11. Geng, G., Myers, R.J., Li, J., Maboudian, R., Carraro, C., Shapiro, D.A., Monteiro, P.J.M.: Aluminum-induced dreierketten chain cross-links increase the mechanical properties of nanocrystalline calcium aluminosilicate hydrate. Sci. Rep. **7**(1), 44032 (2017). https://doi.org/10.1038/srep44032
12. Myers, R.J., L'Hôpital, E., Provis, J.L., Lothenbach, B.: Composition–solubility–structure relationships in calcium (alkali) aluminosilicate hydrate (C–(N,K–)A–S–H). Dalton Trans. **44**(30), 13530–13544 (2015). https://doi.org/10.1039/C5DT01124H
13. Fang, G., Zhang, M.: Multiscale micromechanical analysis of alkali-activated fly ash-slag paste. Cem. Concr. Res. **135**, 106141 (2020). https://doi.org/10.1016/j.cemconres.2020.106141
14. Provis, J.L., Myers, R.J., White, C.E., Rose, V., van Deventer, J.S.J.: X-ray microtomography shows pore structure and tortuosity in alkali-activated binders. Cem. Concr. Res. **42**(6), 855–864 (2012). https://doi.org/10.1016/j.cemconres.2012.03.004
15. Mastali, M., Kinnunen, P., Dalvand, A., Mohammadi Firouz, R., Illikainen, M.: Drying shrinkage in alkali-activated binders—A critical review. Constr. Build. Mater. **190**, 533–550 (2018). https://doi.org/10.1016/j.conbuildmat.2018.09.125
16. Provis, J.L., van Deventer, J.S.J.: Alkali activated materials. State-of-the-Art Report, RILEM TC 224-AAM (Vol. 13, RILEM State-of-the-Art Reports). Springer Dordrecht (2013)
17. Ye, J., Chen, Y., Yan, X.: Influence of load on deformation and strength of fly ash concrete at early age. J. Civil Archit. Environ. Eng. **38**(5), 115–121 (2016). https://doi.org/10.11835/j.issn.1674-4764.2016.05.015
18. Harinadha Reddy, D., Ramaswamy, A.: Experimental and numerical modeling of creep in different types of concrete. Heliyon **4**(7), e00698 (2018). https://doi.org/10.1016/j.heliyon.2018.e00698

19. Han, C., He, Z., Zhan, P., Zhang, X., Wolderufael, Y.F.: Review on effect of mineral admixture on concrete creep. Bull. Chin. Ceram. Soc. **39**(12), 3753–3762 (2020). https://doi.org/10.16552/j.cnki.issn1001-1625.2020.12.002 (in Chinese with English abstract)
20. Wallah, S.E., Hardjito, D.: 10—Assessing the shrinkage and creep of alkali-activated concrete binders. In: Pacheco-Torgal, F., Labrincha, J.A., Leonelli, C., Palomo, A., Chindaprasirt, P. (eds.) Handbook of Alkali-Activated Cements, Mortars and Concretes, pp. 265–290. Woodhead Publishing, Oxford (2015)
21. Sagoe-Crentsil, K., Brown, T., Taylor, A.: Drying shrinkage and creep performance of geopolymer concrete. J. Sustain. Cem.-Based Mater. **2**(1), 35–42 (2013). https://doi.org/10.1080/21650373.2013.764963
22. Davidovits, J.: Geopolymer Chemistry and Applications, 5th edn. Saint-Quentin, France, Institut Géopolymère (2020)
23. Lloyd, R.R., Provis, J.L., Van Deventer, J.S.: Microscopy and microanalysis of inorganic polymer cements. 1: remnant fly ash particles. J. Mater. Sci. **44**, 608–619 (2009). https://doi.org/10.1007/s10853-008-3077-0
24. Gunasekera, C., Setunge, S., Law, D.W.: Creep and drying shrinkage of different fly-ash-based geopolymers. ACI Mater. J. **116**(1), 39–49 (2019). https://doi.org/10.14359/51706941
25. Chao, P., Zheng, J.: Experimental research on creep of self-compacting concrete. Chin. J. Build. Struct. **31**(02), 99–103 (2010). (in Chinese with English abstract)
26. Deng, Z., Xu, H., Li, H., Tong, B., Zhao, S.: Creep law of high-performance concrete. Beijing Gongye Daxue Xuebao/J. Beijing Univ. Technol. **39**(6), 897–901 (2013). (in Chinese with English abstract)
27. Li, J., Yao, Y.: A study on creep and drying shrinkage of high performance concrete. Cem. Concr. Res. **31**(8), 1203–1206 (2001). https://doi.org/10.1016/S0008-8846(01)00539-7
28. Zhang, Y., Wu, X., Bi, Q.: Shrinkage and creep properties of self compacting lightweight aggregate concrete. J. Mater. Sci. Eng. **32**, 35–39 (2014). (in Chinese with English abstract)
29. Zhao, Q., Sun, W., Miao, C., Zheng, K., Liu, J., Lin, W.: Effect of ground granulated blast furnace slag proportion on creep characteristics of concrete. J. Chin. Ceram. Soc. **37**(10), 1760–1766 (2009). (in Chinese with English abstract)
30. Zou, C., Wang, Y., Hu, Q.: Experimental study and model predictive of recycled aggregate concrete creep. J. Wuhan Univ. Technol. **31**(12), 94–98 (2009). https://doi.org/10.3963/j.issn.1671-4431.2009.12.026
31. Zhao, Q., Sun, W., Miao, C., Tian, Q., Zheng, K., Lin, W.: Creep character of high performance concrete with ground granulated blast furnace slag and fly ash. J. Wuhan Univ. Technol. **27**(11), 35–38 (2005). (in Chinese with English abstract)
32. Collins, F.G., Sanjayan, J.G.: Workability and mechanical properties of alkali activated slag concrete. Cem. Concr. Res. **29**(3), 455–458 (1999). https://doi.org/10.1016/S0008-8846(98)00236-1
33. Ma, J., Dehn, F.: Shrinkage and creep behavior of an alkali-activated slag concrete. Struct. Concr. **18**(5), 801–810 (2017). https://doi.org/10.1002/suco.201600147
34. Humad Abeer, M., Provis John, L., Habermehl-Cwirzen, K., Rajczakowska, M., Cwirzen, A.: Creep and long-term properties of alkali-activated Swedish-slag concrete. J. Mater. Civ. Eng. **33**(2), 04020475 (2021). https://doi.org/10.1061/(ASCE)MT.1943-5533.0003381
35. Hu, H., Yu, B., Chen, J.: Development of the high-durability and self-compacting concrete in marine environment. New Build. Mater. 5–8. (in Chinese with English abstract) (2010)
36. Wang, Z., Wang, D.-M.: Influence of different multi-mineral admixtures on long period performance of concrete. Bull. Chin. Ceram. Soc. **34**(8), 2392–2397 (2015). https://doi.org/10.16552/j.cnki.issn1001-1625.2015.08.061
37. Xie, Y., Ma, K., Liu, B., Shi, M.: Creep characteristics of concrete with compound ultra-fine fly ash. J. Chin. Ceram. Soc. **35**(12), 1636–1640 (2007). https://doi.org/10.14062/j.issn.0454-5648.2007.12.015
38. Hojati, M., Rajabipour, F., Radlińska, A.: Creep of alkali-activated cement mixtures. Case Stud. Constr. Mater. **16**, e00954 (2022). https://doi.org/10.1016/j.cscm.2022.e00954

39. Un, C.H.: Creep behaviour of geopolymer concrete, Swinburne University of Technology, Melbourne, Australia (2017). Accessed 4 Oct. 2023. https://researchbank.swinburne.edu.au/file/0ca68717-4117-46f6-b670-03c142d8bbb5/1/chi_hou_un_thesis.pdf
40. Chen, T.-A., Chen, J.-H., Huang, J.-S.: Effects of activator and aging process on the compressive strengths of alkali-activated glass inorganic binders. Cem. Concr. Compos. **76**, 1–12 (2017). https://doi.org/10.1016/j.cemconcomp.2016.11.011
41. He, J., Yang, C.-H.: Hydration heat evolution and setting performance of alkali-slag cement activated with water glass. J. Civil Archit. Environ. Eng. **33**(3), 147–152 (2011). https://doi.org/10.11835/j.issn.1674-4764.2011.03.026
42. Puertas, F., Torres-Carrasco, M.: Use of glass waste as an activator in the preparation of alkali-activated slag. Mechanical strength and paste characterisation. Cem. Concr. Res. **57**, 95–104 (2014). https://doi.org/10.1016/j.cemconres.2013.12.005
43. Islam, M.R.: Creep and shrinkage behavior of fly ash based geopolymer concrete, College of Engineering and Science, Louisina Tech University, Louisina, USA (2015). Accessed 4 Oct. 2023. https://digitalcommons.latech.edu/cgi/viewcontent.cgi?article=1212&context=dissertations
44. Lee, H., Vimonsatit, V., Chindaprasirt, P., Ngo, T., Mendis, P.: Creep properties of cement and alkali activated fly ash materials using nanoindentation technique. Constr. Build. Mater. **168**, 547–555 (2018). https://doi.org/10.1016/j.conbuildmat.2018.02.166
45. Wallah, S., Rangan, B.: Low-calcium fly ash-based geopolymer concrete: long-term properties, Research Report GC 2, Faculty of Engineering, Curtin University of Technology, Perth, Australia (2006). Accessed 4 Oct. 2023. https://www.geopolymer.org/wp-content/uploads/curtin_flyash_GC-2.pdf
46. Castel, A., Foster, S.J., Ng, T., Sanjayan, J.G., Gilbert, R.I.: Creep and drying shrinkage of a blended slag and low calcium fly ash geopolymer concrete. Mater. Struct. **49**(5), 1619–1628 (2016). https://doi.org/10.1617/s11527-015-0599-1
47. Wei, T., Zhao, H., Ma, C.: A comparison of water curing and standard curing on one-part alkali-activated fly ash sinking beads and slag: properties, microstructure and mechanisms. Constr. Build. Mater. **273**, 121715 (2021). https://doi.org/10.1016/j.conbuildmat.2020.121715
48. Athira, V.S., Bahurudeen, A., Saljas, M., Jayachandran, K.: Influence of different curing methods on mechanical and durability properties of alkali activated binders. Constr. Build. Mater. **299**, 123963 (2021). https://doi.org/10.1016/j.conbuildmat.2021.123963
49. Dong, M., Elchalakani, M., Karrech, A.: Curing conditions of alkali-activated fly ash and slag mortar. J. Mater. Civ. Eng. **32**(6), 04020122 (2020). https://doi.org/10.1061/(ASCE)MT.1943-5533.0003233
50. Khan, M.Z.N., Shaikh, Fu.A., Hao, Y., Hao, H.: Effects of curing conditions and sand-to-binder ratios on compressive strength development of fly ash geopolymer. J. Mater. Civ. Eng. **30**(2), 04017267 (2018). https://doi.org/10.1061/(ASCE)MT.1943-5533.0002119
51. Lin, J., Yin, S., Yu, Q., Wen, Z.: Influence of temperature on alkali-activated carbonatite cementitious material. J. Chin. Ceram. Soc. **36**(S1), 197–204 (2008). https://doi.org/10.14062/j.issn.0454-5648.2008.s1.043
52. Wang, X., Zhang, C., Wu, Q., Lin, Y., Zhu, B.: Effect of temperature on the properties of silane coupling agent/geopolymer. Non-Metallic Mines **42**(6), 19–22 (2019). (in Chinese with English abstract)
53. Peng, H., Li, S.-L., Cai, C.-S., Zhang, X.-F., Cui, C.: Study on effect of mix and curing conditions on the mechanical properties and setting time of metakaolin-based geopolymer. Bull. Chin. Ceram. Soc. **33**(11), 2809–2817 (2014). https://doi.org/10.16552/j.cnki.issn1001-1625.2014.11.045
54. Häkkinen, T.: The influence of slag content on the microstructure, permeability and mechanical properties of concrete Part 1 microstructural studies and basic mechanical properties. Cem. Concr. Res. **23**(2), 407–421 (1993). https://doi.org/10.1016/0008-8846(93)90106-J
55. Banthia, N., Gupta, R.: Influence of polypropylene fiber geometry on plastic shrinkage cracking in concrete. Cem. Concr. Res. **36**(7), 1263–1267 (2006). https://doi.org/10.1016/j.cemconres.2006.01.010

56. Noushini, A., Castel, A., Gilbert, R.I.: Creep and shrinkage of synthetic fibre-reinforced geopolymer concrete. Mag. Concr. Res. **71**(20), 1070–1082 (2019). https://doi.org/10.1680/jmacr.18.00053
57. Zhao, Q., Yu, J., Geng, G., Jiang, J., Liu, X.: Effect of fiber types on creep behavior of concrete. Constr. Build. Mater. **105**, 416–422 (2016). https://doi.org/10.1016/j.conbuildmat.2015.12.149
58. Ji, G.M., Kanstad, T., Bjøntegaard, Ø., Sellevold, E.J.: Tensile and compressive creep deformations of hardening concrete containing mineral additives. Mater. Struct. **46**(7), 1167–1182 (2013). https://doi.org/10.1617/s11527-012-9962-7
59. Hilaire, A., Benboudjema, F., Darquennes, A., Berthaud, Y., Nahas, G.: Modeling basic creep in concrete at early-age under compressive and tensile loading. Nucl. Eng. Des. **269**, 222–230 (2014). https://doi.org/10.1016/j.nucengdes.2013.08.034
60. Rossi, P., Charron, J.P., Bastien-Masse, M., Tailhan, J.-L., Le Maou, F., Ramanich, S.: Tensile basic creep versus compressive basic creep at early ages: comparison between normal strength concrete and a very high strength fibre reinforced concrete. Mater. Struct. **47**(10), 1773–1785 (2014). https://doi.org/10.1617/s11527-013-0150-1
61. Li, Z., Zhang, S., Liang, X., Ye, G.: Cracking potential of alkali-activated slag and fly ash concrete subjected to restrained autogenous shrinkage. Cem. Concr. Compos. **114**, 103767 (2020). https://doi.org/10.1016/j.cemconcomp.2020.103767
62. Klausen, A.E., Kanstad, T., Bjøntegaard, Ø., Sellevold, E.: Comparison of tensile and compressive creep of fly ash concretes in the hardening phase. Cem. Concr. Res. **95**, 188–194 (2017). https://doi.org/10.1016/j.cemconres.2017.02.018
63. Cheng, Z., Zhao, R., Yuan, Y., Li, F., Castel, A., Xu, T.: Ageing coefficient for early age tensile creep of blended slag and low calcium fly ash geopolymer concrete. Constr. Build. Mater. **262**, 119855 (2020). https://doi.org/10.1016/j.conbuildmat.2020.119855
64. Zhou, X., Wang, Y., Zheng, W., Chen, P., Zeng, Y.: Effect of stress–strength ratio on creep property of sodium silicate–based alkali-activated slag concrete. Appl. Sci. **9**(18), 3643 (2019). https://doi.org/10.3390/app9183643
65. Bažant, Z.P., Hauggaard Anders, B., Baweja, S., Ulm, F.-J.: Microprestress-solidification theory for concrete creep. I: aging and drying effects. J. Eng. Mech. **123**(11), 1188–1194 (1997). https://doi.org/10.1061/(ASCE)0733-9399(1997)123:11(1188)
66. Ye, H., Radlińska, A.: Shrinkage mechanisms of alkali-activated slag. Cem. Concr. Res. **88**, 126–135 (2016). https://doi.org/10.1016/j.cemconres.2016.07.001
67. Li, Z., Lu, T., Liang, X., Dong, H., Ye, G.: Mechanisms of autogenous shrinkage of alkali-activated slag and fly ash pastes. Cem. Concr. Res. **135**, 106107 (2020). https://doi.org/10.1016/j.cemconres.2020.106107
68. Abate, S.Y., Park, S., Kim, H.-K.: Parametric modeling of autogenous shrinkage of sodium silicate-activated slag. Constr. Build. Mater. **262**, 120747 (2020). https://doi.org/10.1016/j.conbuildmat.2020.120747
69. Wang, J., Lu, P., Xu, Q., Luo, X., Zhu, M.: Calculation model for concrete creep and its practical application. Eng. Mech. **35**(1), 156–160 (2018). https://doi.org/10.6052/j.issn.1000-4750.2018.01.S029
70. Zheng, Z., Liu, H., Xiao, M., He, J., Xie, H., Zhuo, L.: A creep model coupling moisture and mechanical damage for water-bearing concrete. Constr. Build. Mater. **326**, 126598 (2022). https://doi.org/10.1016/j.conbuildmat.2022.126598
71. Wu, F., Yu, Q., Liu, C.: Creep characteristics and constitutive model of bio-based concrete in aqueous environment. Constr. Build. Mater. **320**, 126213 (2022). https://doi.org/10.1016/j.conbuildmat.2021.126213
72. EN 1992-1-1:2004/A1.: Eurocode 2: Design of concrete structures—Part 1-1: general rules and rules for buildings. European Committee for Standartization, Brussels, Belgium
73. Wallah, S.E.: Creep behaviour of fly ash-based geopolymer concrete. Civil Eng. Dimens. **12**(2), 73–78 (2010). https://doi.org/10.9744/ced.12.2.73-78
74. Gilbert, R.I.: Creep and shrinkage models for high strength concrete—Proposals for inclusion in AS3600. Aust. J. Struct. Eng. **4**(2), 95–106 (2002). https://doi.org/10.1080/13287982.2002.11464911